Activation of Adaptive and Innate Immune Cells via Localized IL2 Cytokine Factories Eradicates Mesothelioma Tumors

Amanda M. Nash[1], Samira Aghlara-Fotovat[1], Bertha Castillio[1], Andrea Hernandez[1], Aarthi Pugazenthi[2], Hyun-Sung Lee[2], Hee-Jin Jang[2], Annie Nguyen[1], Alexander Lu[1], Bryan M. Burt[2], Ravi K. Ghanta[2], and Omid Veiseh[1]

ABSTRACT

Purpose: IL2 immunotherapy has the potential to elicit immune-mediated tumor lysis via activation of effector immune cells, but clinical utility is limited due to pharmacokinetic challenges as well as vascular leak syndrome and other life-threatening toxicities experienced by patients. We developed a safe and clinically translatable localized IL2 delivery system to boost the potency of therapy while minimizing systemic cytokine exposure.

Experimental Design: We evaluated the therapeutic efficacy of IL2 cytokine factories in a mouse model of malignant mesothelioma. Changes in immune populations were analyzed using time-of-flight mass cytometry (CyTOF), and the safety and translatability of the platform were evaluated using complete blood counts and serum chemistry analysis.

Results: IL2 cytokine factories enabled 150× higher IL2 concentrations in the local compartment with limited leakage into the systemic circulation. AB1 tumor burden was reduced by 80% after 1 week of monotherapy treatment, and 7 of 7 of animals exhibited tumor eradication without recurrence when IL2 cytokine factories were combined with anti–programmed cell death protein 1 (aPD1). Furthermore, CyTOF analysis showed an increase in $CD69^{+}CD44^{+}$ and $CD69^{-}CD44^{+}CD62L^{-}$ T cells, reduction of $CD86^{-}$PD-$L1^{-}$ M2-like macrophages, and a corresponding increase in $CD86^{+}$PD-$L1^{+}$ M1-like macrophages and MHC-II^{+} dendritic cells after treatment. Finally, blood chemistry ranges in rodents demonstrated the safety of cytokine factory treatment and reinforced its potential for clinical use.

Conclusions: IL2 cytokine factories led to the eradication of aggressive mouse malignant mesothelioma tumors and protection from tumor recurrence, and increased the therapeutic efficacy of aPD1 checkpoint therapy. This study provides support for the clinical evaluation of this IL2-based delivery system.

See related commentary by Palanki et al., p. 5010

Introduction

Malignant mesothelioma affects the organs that are lined by the mesothelium, including the organs of the chest (pleura) and abdomen (peritoneum). It is a highly aggressive cancer and is essentially lethal in all cases (1–5). The most common etiology of this disease is industrial/environmental exposure to asbestos (∼80%), although it can result from radiation and is occasionally idiopathic (6–8). The combination of pemetrexed and cisplatin treatment was determined to be the first-line chemotherapy for malignant mesothelioma. However, this regimen only increased median survival from 9 to 11.4 months, compared with cisplatin alone (9). More recently, the antiangiogenic agent bevacizumab increased survival by 2 months when added to pemetrexed/cisplatin (10). Radiation is limited by the large size of its required field, and it is ineffective as a primary treatment (11–14). In those with early-stage disease, adding surgery can improve median survival to 14–19 months (1, 15, 16). However, surgery is associated with significant morbidity, 3%–10% operative mortality, and early local recurrence (1, 15, 17–22). In recent trials, immune checkpoint inhibitors such as nivolumab or pembrolizumab have shown encouraging clinical activity and good tolerability in patients with advanced malignant pleural mesothelioma (23, 24). Objective response rates (ORR) ranged from 15% to 21%, and rates of stable disease (SD) ranged from 33% to 56%, equating to 53% of patients experiencing durable clinical benefit (DCB; i.e., ORR+SD; refs. 23, 25–28). These results led to its recent approval by the FDA as the first line of defense for malignant pleural mesothelioma (29, 30). Despite promising clinical results, optimal and safe delivery remains a challenge (31). Side effects of immune checkpoint inhibitors are predominantly immunologic, and immune adverse events (iAE) occur in 74% of patients receiving PD-1 inhibitors, 14% of which are grade III–IV iAEs (32). Local drug delivery can reduce toxicity by confining the immunostimulatory effects to the tumor microenvironment, highlighting a strong rationale for developing such approaches (33).

IL2 is a proinflammatory cytokine that is critical for the activation, differentiation, and survival of T and NK cells and helps recruit immune cells to the tumor microenvironment (34). While the use of this cytokine was initially introduced as a systemic therapy and led to 20% objective response rates (ORR), its widespread activation of circulating T cells resulted in severe toxicity and the production of excess inflammatory cytokines, a phenomenon often referred to as cytokine storm. Nevertheless, the discovery of IL2 was a breakthrough in cancer immunotherapy, and it has since been demonstrated that local IL2 may be similarly efficacious but less toxic due to its confined action on tumor-adjacent effector immune cells (35). In addition, the IL2 concentrations that are able to be achieved with local administration enable more efficient activation of antitumor immunity,

[1]Department of Bioengineering, Rice University, Houston, Texas. [2]Michael E. DeBakey Department of Surgery, Baylor College of Medicine, Houston, Texas.

A.M. Nash and S. Aghlara-Fotovat contributed equally to this article.

Corresponding Author: Omid Veiseh, Rice University, 6500 Main St., Houston, TX 77030. Phone: 713-348-3082; E-mail: omid.veiseh@rice.edu

Clin Cancer Res 2022;28:5121–35

doi: 10.1158/1078-0432.CCR-22-1493

Translational Relevance

IL2 is one of two FDA-approved cytokine therapies for cancer treatment and plays a critical role in the activation of the immune system. In this study, we utilized a mouse model of malignant mesothelioma and demonstrated the ability to eradicate these tumors with IL2 cytokine factories. The rapid clinical course of malignant mesothelioma necessitates the development of highly effective treatment modalities that are safe and fast-acting. IL2 immunotherapy allows for rapid activation of tumor-adjacent effector T cells, which leads to the destruction of tumor cells as well as the development of memory T cells for protection against recurrence. For this reason, IL2 cytokine factories have the potential to be transformative for patients who have not responded well to combination chemotherapy or other immunotherapies, such as immune checkpoint inhibitors. Furthermore, because IL2 treatment has been shown to induce memory T-cell formation, this platform also is promising for patients with tumor recurrence.

necessitating lower doses. Several clinical studies have evaluated intrapleural infusions of IL2 for the treatment of malignant pleural mesothelioma, and the results showed improvements in ORR and disease control rate (DCR) (36–38). Importantly, local intrapleural IL2 infusions facilitated IL2 levels 6000-fold higher than systemic levels resulting in therapeutic efficacy without causing systemic toxicities typically associated with intravascularly administered IL2 therapy (36). However, the need for continuous infusion and large administration volumes (>100 mL throughout treatment) necessary for this approach led to complications such as catheter infection that have prevented widespread use (36–39). Combined, these studies highlight that an approach for continuous local administration of IL2 could significantly improve immunotherapy for patients with malignant mesothelioma (40).

We recently developed a localized cell-based immunotherapy for improved delivery of IL2 using immunostimulatory alginate-based microparticles (41). Using this system, which we call RPE-mIL2 cytokine factories, we can deliver high concentrations of IL2 locally while maintaining low systemic concentrations, alleviating the risk of toxicity. Previously, we demonstrated the therapeutic potential of this platform in mouse models of ovarian and colorectal cancers and developed a clinical-grade version of this product (AVB-001) which is now advancing toward a phase I human clinical trial in platinum-resistant ovarian cancer patients. AVB-001 also has significant potential to treat mesothelioma tumors. In this study, we used our IL2 cytokine factory platform in the highly aggressive AB1 malignant mesothelioma mouse model. Using this system, we successfully eradicated the malignant mesothelioma tumor burden in all treated mice. Significantly, this approach was used in combination with the FDA-approved checkpoint inhibitor, aPD1, and improved its therapeutic efficacy. The results of this study present justification for the initiation of a clinical trial that evaluates local administration of IL2 cytokine factories as a monotherapy or in combination with aPD1 for the treatment of malignant mesothelioma.

Materials and Methods

Cell culture and engineering

Cell culture media and associated reagents were purchased through Fisher Scientific. Transfection reagents (Lipofectamine 3000) and selection media (puromycin) were purchased from Invitrogen. Expression vectors and helper plasmids were designed and purchased through VectorBuilder. Live Dead stains (Fisher Scientific) were used to determine cell viability of encapsulated cells. All cell lines tested negative for mycoplasma contamination. Cell lines used in our studies were authenticated by the vendor.

These cells were cultured using Dulbecco's Modified Eagle Medium (DMEM/F-12), with 10% FBS and 1% antibiotic-antimycotic (AA). The media were changed three times weekly. Media used for AB1 cells was RPMI1640, 10% FBS, and 1% antibiotic–antimycotic (AA). All cells were passaged at least twice between thawing and collection in the studies described here.

Cell transfection/transduction

ARPE-19 cells (ATCC) were engineered to express cytokines of interest. AB1 cells (Sigma-Aldrich) were engineered to express firefly luciferase. Cells were transfected or transduced as described previously (41).

Core shell cell encapsulation

Capsules were generated as described previously (42). Briefly, alginate was dissolved at 1.4% w/v in saline and sterile filtered. Cells were resuspended in alginate at a concentration of 42×10^6 cells/mL. Encapsulation occurred using a custom-built, two-fluid co-axial electrostatic spraying device. Alginate droplets were expelled from a co-axial needle into barium chloride crosslinking solution where they formed hydrogel capsules. They were subsequently washed with HEPES buffer and maintained with normal cell culture techniques.

Cell viability postencapsulation

Following encapsulation, a subset of capsules were washed with 5 mL DPBS and stained using a stock 2 μmol/L calcein AM and 4 μmol/L EthD-1 in DPBS. The sample was incubated for 20 minutes and imaged using a fluorescence microscope.

ELISA

An individual capsule was added to a 96 well plate ($n = 5$–8) in 200 μL for 24 hours at 37 degrees in a 5% CO2 humidified atmosphere. Cell supernatant was collected from each well and assayed via ELISA according to manufacturer protocols. Kits were obtained commercially for mouse IL2 (R&D Systems) and human IL2 (R&D Systems). All samples were run in triplicate.

CyTOF experiments

Single cells were stabilized for 6 hours in media at 37°C. A total of 5×10^5 cells were resuspended in Maxpar Cell Staining Buffer (Fluidigm, catalog no.201068) in individual 5-mL tubes for each sample to be barcoded. Mass-tag cellular barcoding using the Cell-ID 20-Plex Pd Barcoding Kit (Fluidigm, catalog no. 201060) was performed. Cell-ID Intercalator-Ir is a cationic nucleic acid intercalator that contains naturally abundant Iridium (191Ir and 193Ir) and is used for identifying nucleated cells in CyTOF analysis according to standard protocol. For measurement of intracellular cytokines by CyTOF, cells harvested from mice were incubated in 1 μL/mL Golgistop (BD cell analysis, catalog no. BD B554724A) for 10 hours at 37°C, according to standard protocol. The samples were then washed and incubated with cell surface antibodies for 45 minutes on ice and washed. After overnight incubation at 4°C with resuspension in 1× Fix I buffer, the samples were stained with intracellular antibodies against cells cytokines for 30 minutes at room temperature and washed. Stained cells were analyzed on a mass cytometer (CyTOF3 mass cytometer,

Fluidigm) at an event rate of 400 to 500 cells per second. All mass cytometry files were normalized together using the mass cytometry data normalization algorithm, which uses the intensity values of a sliding window of these bead standards to correct for instrument fluctuations over time and between samples. Barcodes were deconvoluted using the Debarcoder software (Fluidigm).

CyTOF analysis

Total live nucleated cells were used for all analyses and visualized using the UMAP for dimensional reduction (43). 40,000 immune cells were downsampled from each sample, and they were integrated into one file. Acquired single-cell data were transferred into additional cytometric analysis in FlowJo V10 software (FlowJo, LLC). To characterize all cells obtained from peritoneal lavage fluids, all cells, were organized in 14 phenotypes. Fourteen cellular phenotypes were manually defined by a panel of 43 antibodies (Supplementary Table S1): memory B cells (CD45+CD19+B220+CD86+), naïve B cells ($CD45^+CD19^+B220^+CD86^-$), active CD4 T cells ($CD45^+CD3^+$ $TCR\text{-}\beta^+CD4^+CD44^+CD69^+CD62L^-$), effector memory CD4 T cells ($CD45^+CD3^+TCR\text{-}\beta^+CD4^+CD44^+CD69^-CD62L^-$), naïve CD4 T cells ($CD45^+CD3^+TCR\text{-}\beta^+CD4^+CD44^-CD69^-CD62L^+$), active CD8 T cells ($CD45^+CD3^+TCR\beta^+CD8^+CD44^+CD69^+CD62L^-$), effector memory CD8 T cells ($CD45^+CD3^+TCR\beta^+CD8^+CD44^+$ $CD69^-CD62L^-$), naïve CD8 T cells ($CD45^+CD3^+TCR\text{-}\beta^+CD8^+$ $CD44^-CD69^-CD62L^+$), γδT cells ($CD45^+CD3^+TCR\beta^-$), M1-like macrophages ($CD45^+CD3^-CD64^+F4/80^+CD86^+PD\text{-}L1^+$), M2-like macrophages ($CD45^+CD3^-CD64^+F4/80^+CD86^-PD\text{-}L1^-$), plasmacytoid dendritic cells ($CD45^+CD3^-CD19^-CD11c^+B220^+CD317^+$), conventional DC ($CD45^+CD3^-CD19^-CD11c^+B220^-MHCII^+$). Mapping of our data onto its interface enabled visualization and precise quantification of immune cells in any sample as a UMAP plot, and generation of separate maps for defined groups of mice enables comparison of cellular networks between these groups. To improve efficiency and ease of display of our multiple proposed experiments, we generated the intuitive single-cell maps for each comparison (as in **Fig. 3**). Cell frequencies or proportions were compared across groups of interest. On the basis of the outcome of interest, statistically significant changes in cell frequencies for each cluster were shown in a single map with the directionality of change given by color. Mean metal intensities (MMI) of proteins were used to evaluate the expression of cytokines and immunoregulatory proteins.

Animal studies

Mouse studies

Balb/C mice (Charles River Laboratories), a mixture of males and females, aged 8–10 weeks were used for *in vivo* studies. All animal experiments were approved by Rice University's Institutional Animal Care and Use Committee (IACUC). All biological samples implanted into animals were approved by Rice University's Institutional Biosafety Committee (IBC). For IP tumor models of AB1-Fluc; 5×10^5 cells suspended in HBSS were intraperitoneally injected to the lower right abdomen. Tumors were injected and allowed to develop *in vivo* for 1 week before treatment (**Figs. 1E–K** and **2B–G**; Supplementary Figs. S2A–S2C and S5A–S5B). For all studies using *in vivo* imaging system (IVIS) imaging for tumor growth tracking, mice were imaged and stratified into treatment groups 1 day prior to surgery using the methods described in IVIS imaging section below (**Figs. 1E** and **2B**; Supplementary Figs. S2A, S5A and S5B). After stratification for tumor size, animals were randomly assigned to treatment groups. For tumor measurements, experimenters were not blinded (as it is commonly accepted in the field). Antitumor efficacy of therapy was confirmed by multiple investigators.

Experimental controls

Sham: All mice given sham surgery received IP surgery and were administered 1 mL sterile saline.

RPE: RPE capsules contained the same density of cells as experimental capsules but contained naïve cells.

aPD1: All mice treated with aPD1 antibodies (J43, BioXcell) received intraperitoneal injection of 200 μg per mouse at day 0, 3, 7, and 10 posttreatment.

Subcutaneous tumor growth tracking

For subcutaneous AB1 rechallenge models, the tumor size was measured using a digital caliper and tumor volume was calculated using the formula $V = 0.5 \times (\text{height}) \times (\text{width}^2)$.

For rechallenge experiments, 5×10^5 AB1 cells suspended in HBSS were injected subcutaneously into the rear flank of Balb/C mice that showed complete remission from intraperitoneal tumor inoculations (**Fig. 2I–J**).

Immune cell depletion studies

For depletion studies (Supplementary Fig. S2A–S2C), isotype control (LTF-2), anti-CD8α (2.43), or anti-CD4 (GK1.5) antibodies (BioXcell) were administered via intraperitoneal injection at a dose of 100 μg per animal at day -2, 0, and 2 post RPE-mIL2 implantation.

Intraperitoneal tumor growth tracking

Animals injected with AB1-Fluc cells were imaged using IVIS 6 days after injection and stratified into experimental groups based on luminescent signal. After surgery, animals were tracked for tumor growth or reduction using IVIS imaging 1x per week. Imaging methods are expanded below.

Intraperitoneal surgical implantation of capsules in mice

Implantation studies were carried out as previously described (41). Briefly, mice were sedated and anaesthetized in accordance with approved animal protocols at Rice University. A surgical blade (15T; Sklar) was then used to cut a 0.5–0.75 cm midline incision through the skin and the linea alba into the abdomen. Capsule implants were administered using sterile transfer pipettes. The abdominal muscle was closed by suturing with 5–0 Ethicon black PDS-absorbable or other 5.0–6.0 monofilament absorbable sutures. The external skin layer was closed with PDS suture as previously described.

IVIS imaging

Mice were anaesthetized in accordance with approved animal protocols at Rice University and injected in the IP space with D-luciferin (300 μg/mL, 200 μL; PerkinElmer). Animals were then transferred to the IVIS manifold (IVIS Spectrum, PerkinElmer) where they were kept under isoflurane anesthesia (0.25 L/minute) and maintained warm on a heated stage. Photographs and luminescent images were acquired 10 minutes after injection. Luminescent exposures were set to 1 second with the binning set at medium, the excitation set to block, the EM gain set to "off" with 0-second delays between acquisitions. Subsequent to stratification, the image of each mouse was individually cropped and stitched to create a collage of each treatment group.

H&E staining of explanted capsules

Post retrieval, extracted capsules were rinsed three times with PBS and fixed in 10% formalin overnight. After fixation, the samples were

rinsed twice with PBS, and dehydrated in gradually ascending ethanol solutions for 20 minutes each time. The samples were cleared in xylene for 10 minutes, and incubated in a 50/50 solution of xylene and paraffin overnight at 57°C. On day 3, the samples were transferred to paraffin twice for 1 hour each, and then embedded in a paraffin mould. Subsequently, embedded samples were sectioned at 5-μm thickness onto positively charged lysine microscope slides. Tissue sections were then stained for H&E to assess pericapsular cellular overgrowth.

Rat studies

Sprague Dawley rats were purchased from Envigo. Animals were anesthetized with inhalational isoflurane in 100% O_2 (5.0% induction; 2.5% maintenance). Endotracheal intubation was performed, and the animals ventilated with positive-pressure ventilation. A left lateral thoracotomy was performed. Capsules were deposited directly into the pleural cavity via Pasteur pipette and a total transfer volume of 300 μL. Each animal received one dose of 65 capsules. The chest was then sutured closed in layers and the animals were extubated and allowed to recover.

Toxicity analyses

At the scientific endpoint, rats were anesthetized and 2 mL of blood was collected from the inferior vena cava prior to euthanasia. Samples were submitted to the Mouse Metabolism and Phenotyping Core at Baylor College of Medicine. Both a Diabetes and Lipid panel, as well as a Liver panel were acquired.

Histology

At the scientific endpoint, rat hearts were perfused with PBS and excised. Lungs, liver, kidneys, and spleen were also excised. Each of the organs was fixed in 10% formalin. Formalin was exchanged for 70% ethanol after 24 hours. Organs were submitted to the Pathology Core and Lab where 5um tissue sections were cut and H&E stained at 0, 300, and 600 μm deep into each tissue.

Statistical analysis

Sample size was predetermined from pilot experiments and/or experiments that have been done in the past, to obtain statistically significant data. Experiments were repeated at least once, or data were compiled from two independent experiments unless otherwise stated in the respective figure legend. Replicates were reproducible. All statistical analyses were conducted using GraphPad Prism 9. One-way ANOVA tests with the Holm–Sidak multiple comparisons methods were used to determine *P* values for CyTOF datasets and toxicity assays. Unless otherwise indicated as a replicate measurement, data were taken from distinct samples.

Data availability

All data needed to evaluate the conclusions in the article are present in the article and/or the Supplementary Materials. The datasets generated during and/or analysed during the current study are available from the corresponding author on reasonable request.

Results

IL2-based cytokine factories result in dose-dependent regression of AB1 tumors in mice

Our IL2-based delivery system consisted of polymer encapsulated human retinal pigmented epithelial (RPE) cells that were engineered to stably express human or mouse IL2 (**Fig. 1A**) using the PiggyBAC transposon system. These xenogeneic engineered cells were then protected from the host immune system via hydrogel microencapsulation (**Fig. 1A**) as previously described (42). After encapsulation, the engineered cells continue to secrete IL2 and the cytokine molecules escape from the pores of the hydrogel via diffusion. Following encapsulation, the IL2-based cytokine factories are referred to as RPE-mIL2 (mouse IL2) or RPE-hIL2 (human IL2).

Precise IL2 dosing is critical for successful immune cell activation without triggering toxicity. For this reason, we designed our delivery system with two levels of dose modulation. First, the administered IL2 concentration can be altered by changing the density of engineered cells suspended in each capsule. Second, the dose can be fine-tuned by changing the number of individual capsules in a given dose. To test our hypothesis, we fabricated IL2-based cytokine factories at three different cell densities and assayed individual capsules from each dose group for IL2 production. Next, we varied the number of capsules in each dose and evaluated the dose-dependent anti-tumor response in mice with AB1 tumors. Our results demonstrate that as the cell concentration per capsule increases (Supplementary Fig. S1A), the concentration of IL2 from an individual capsule also increases (**Fig. 1B**) without reducing cell viability within the capsules (**Fig. 1C**), providing dose-dependent control.

To evaluate whether anti-tumor efficacy was also dose-dependent, we utilized an intraperitoneal mouse model of mesothelioma and administered various doses of RPE-mIL2 according to the experimental timeline seen in **Fig. 1D**. Notably, we found that increasing the number of capsules in each dose also provides a dose dependent anti-tumor effect in mice bearing AB1 tumors (**Fig. 1E**). Tumor regression was not seen in the control animals at any time (**Fig. 1F** and **G**). After one week of RPE-mIL2 treatment we saw tumor reduction by greater than 45% percent, regardless of the dose, in 19 of 26 mice when compared to the total flux before treatment (**Fig. 1H–K**). Notably, 11/12 mice treated with at least 2.5 μg of RPE-mIL2 had greater than 75% reduction in tumor burden in one week and 100% of mice treated with 5 μg of RPE-mIL2 had 90% reduction in tumor burden. Mice in the sham and capsule control (RPE) groups experienced progressive tumor growth over time (**Fig. 1F** and **G**) while mice treated with RPE-mIL2 experienced tumor regression and extended survival (**Fig. 1H–K**). Furthermore, 17 of 19 mice treated with at least 1.5 μg of RPE-mIL2 survived more than 2x longer than mice in the sham group. Importantly, we did not observe any significant deviations in body weight over time in any of the treatment groups suggesting that the therapy was well tolerated (Supplementary Fig. S1B–S1E). These results highlight the significant anti-tumor effects of RPE-mIL2 treatment in mice with AB1 tumors.

To understand when this therapy would be most beneficial to patients, we additionally evaluated the ability of our mIL2 cytokine factories to eradicate more aggressive tumors. Mice were injected intraperitoneally with AB1 cells and were treated on day 11 with 5 μg of RPE-mIL2. Treatment at this timepoint did not result in tumor eradication, however, it did result in a significant reduction in tumor burden compared to sham 1 week after treatment ($P < 0.01$; Supplementary Fig. S1F).

$CD8^+$ cytotoxic T cells are required for RPE-mIL2–based antitumor responses seen in AB1 tumor-bearing mice

IL2 is known to be a potent activator and inducer of the proliferation of effector T cells (44). To elucidate whether $CD8^+$ or $CD4^+$ T-cell populations (or both) were required to reproduce the tumor reduction

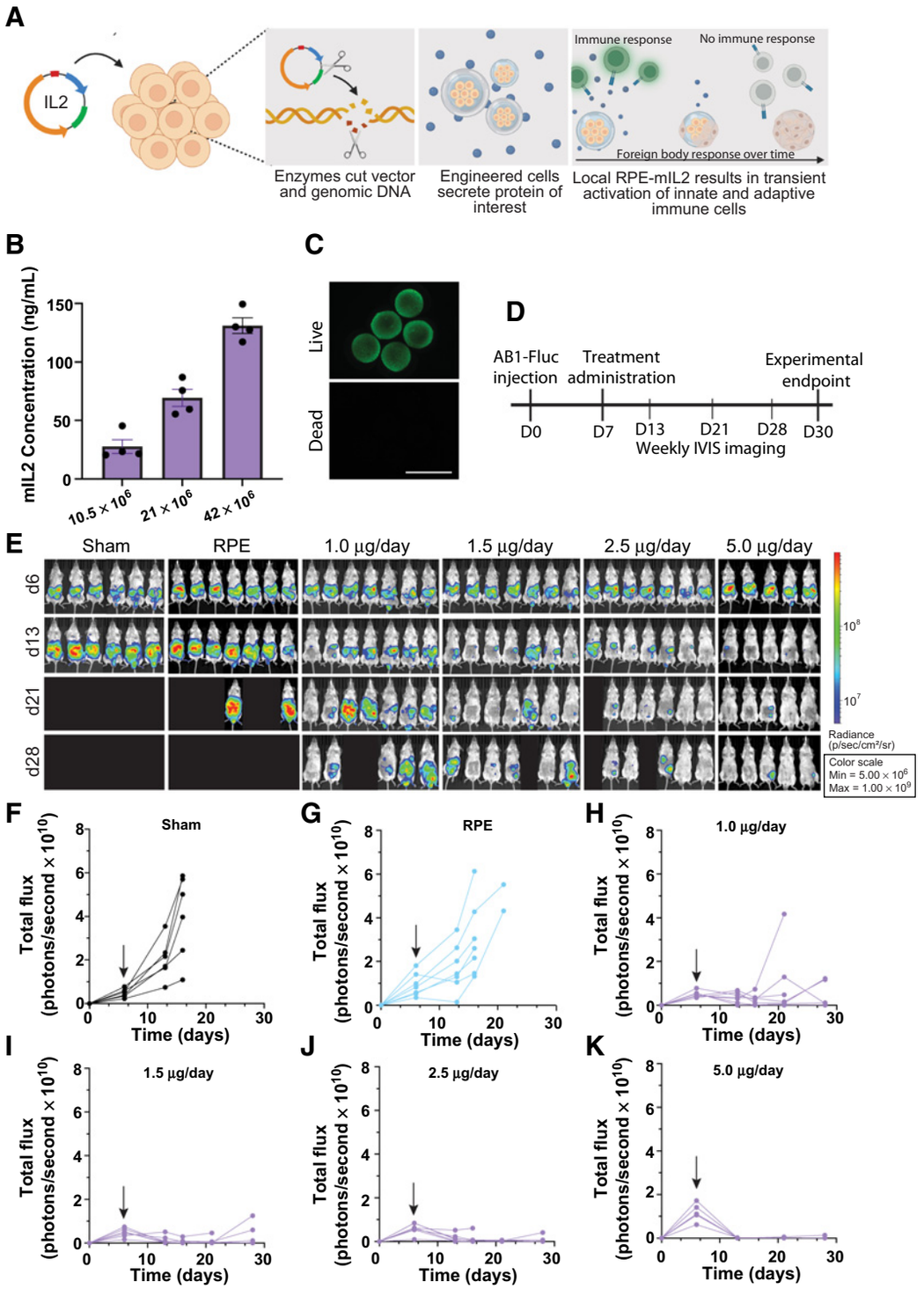

Figure 1.

Dose response of RPE-mIL2 in a peritoneal model of malignant mesothelioma. **A,** Schematic demonstrating the development of RPE-mIL2 cells and encapsulation in hydrogel spheres. **B,** ELISA measurements of mIL2 in supernatant collected from capsules after 24 hours of *in vitro* culture. **C,** Representative live/dead image of RPE-mIL2 cells encapsulated at 42 × 10^6 cells/mL in alginate. **D,** Schematic illustrating the experimental timeline for tumor establishment, treatment, and IVIS imaging. **E,** Luminescent images tracking AB1-FLuc tumor burden over time beginning at day 6 post injection, and weekly until day 28 post injection. Subsequent to stratification, the image of each mouse was individually cropped and stitched to create a collage of each treatment group. **F–K,** Quantification of tumor burden for each treatment group (n = 5–7) represented by total flux (photons/second) plotted over time. Black arrows indicate the day of treatment administration.

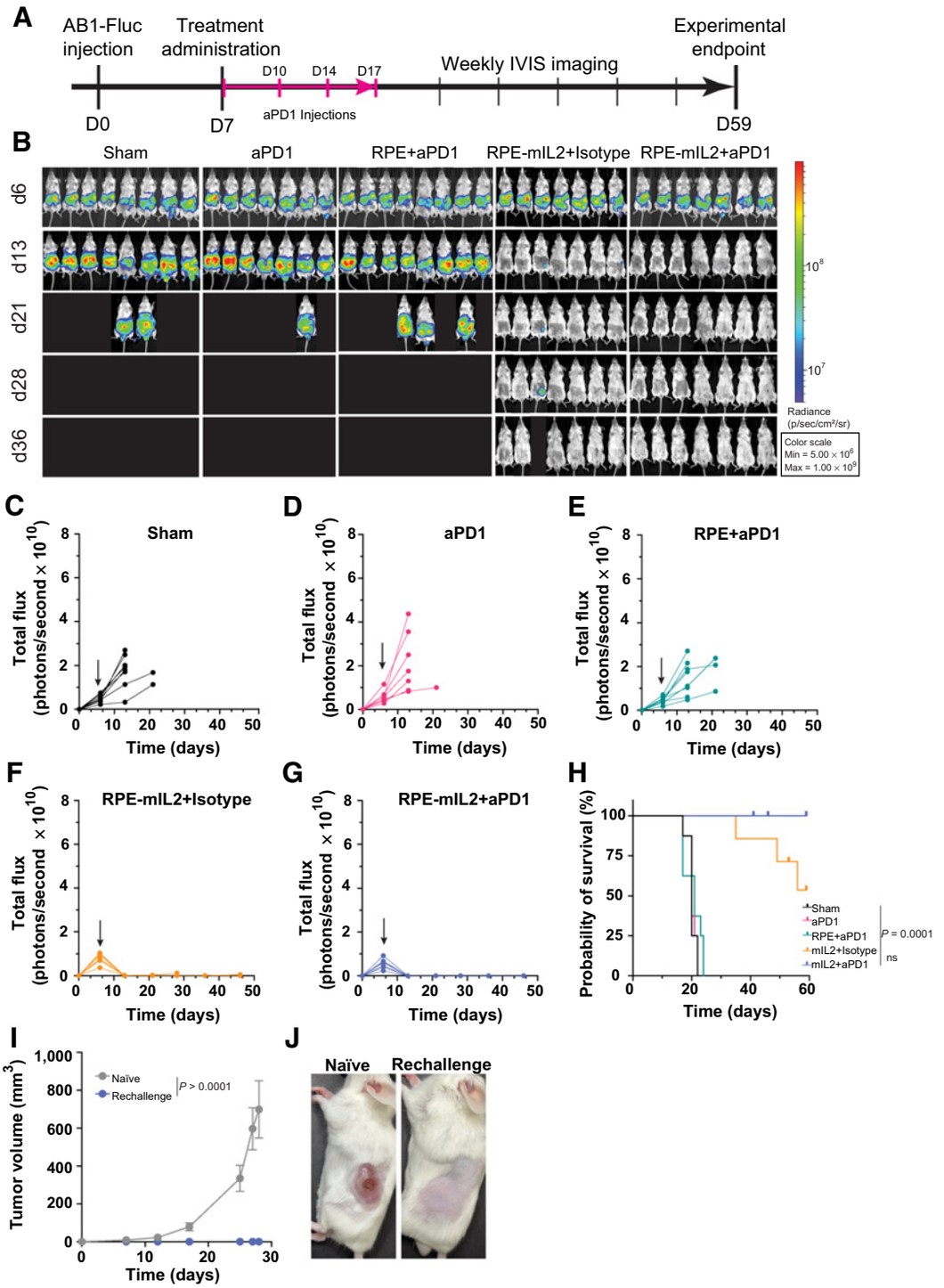

Figure 2.

RPE-mIL2 improves therapeutic efficacy of aPD1. **A,** Schematic of the experimental timeline for tumor establishment, treatment administration, and IVIS imaging. **B,** Luminescent images tracking tumor burden over time. Subsequent to stratification, the image of each mouse was individually cropped and stitched to create a collage of each treatment group. **C–G,** Quantification of tumor burden for each treatment group ($n = 7–8$) represented by total flux (photons/second) plotted over time. Black arrows indicate the day of treatment administration. **H,** Survival curves plotted as percent survival over time beginning after tumor injection ($n = 7–8$). *P* value was determined by a comparison of survival curves by the log-rank (Mantel–Cox) test (ns = not significant). **I,** plot of subcutaneous tumor volume over time in naïve mice compared with RPE-mIL2+aPD1–treated mice. *P* values were acquired using one-way ANOVA with Holm–Sidak method for multiple comparisons. **J,** Representative macroscopic images of the left flank 28 days post subcutaneous tumor injection. (Left; naïve, Right; RPE-mIL2+aPD1 treated).

seen in our earlier studies, we utilized antibodies against $CD8^+$ or $CD4^+$ T cells in AB1 tumor-bearing mice treated with RPE-mIL2. As expected, mice lacking $CD8^+$ T cells were unable to mount a sufficient antitumor response after treatment. The average total flux from this group was comparable to mice in the sham and RPE control groups after one week of treatment (Supplementary Fig. S2A and S2B). However, the $CD4^+$ T cell-depleted mice showed an antitumor response which was similar to the immune-competent mice after RPE-mIL2 treatment, suggesting that $CD4^+$ T cells are not required to mount an antitumor response with our treatment (Supplementary Fig. S2A and S2B). This trend was consistent throughout the study and seen in Supplementary Fig. S2C–S2G where the total flux from RPE-mIL2, RPE-mIL2+isotype and RPE-mIL2+anti-CD4–treated mice all exhibit decreases in tumor flux while sham and RPE-mIL2+anti-CD8 treated mice exhibit progression of tumor growth over time. Taken together, these data provide mechanistic insight into the immune cells responsible for antitumor efficacy after RPE-mIL2 treatment and suggest that our results are largely $CD8^+$ T cell–dependent.

RPE-mIL2 in combination with aPD1 checkpoint therapy eradicates AB1 tumor burden and provides protection against recurrence in mice

Checkpoint therapy has currently become available as first-line therapy for patients with unresectable malignant mesothelioma; however, response rates are still limited (45). To evaluate the potential of RPE-mIL2 to increase the efficacy of checkpoint inhibitors, we conducted a combination study with RPE-mIL2 and aPD1 treatment. The experiment was carried out according to the schematic seen in **Fig. 2A**. AB1 tumors in the intraperitoneal space of the 7 of 7 mice treated with RPE-mIL2+aPD1 were eradicated after one week of treatment and did not recur throughout the duration of the study (**Fig. 2B**). In addition, 7 of 7 mice treated with RPE-mIL2+isotype experienced a significant reduction of tumor burden early on and tumors in 5 of 7 of these mice were eradicated. Significantly, mice treated with sham surgical control, PD-1 only, or RPE+aPD1 did not experience tumor regression at any time during the study and 100% of these control mice reached humane endpoints for euthanasia within three weeks after tumor administration (**Fig. 2B–G**). The total flux of each animal in this study was plotted over time. Mice in each of the control groups experienced increases in total flux until they reached humane endpoints and were euthanized (**Fig. 2B–E**). Mice treated with RPE-mIL2+isotype or RPE-mIL2+aPD1 never experienced a total flux higher than the starting value suggesting strong antitumor efficacy after RPE-mIL2 treatment (**Fig. 2B**, **F** and **G**). Notably, mice treated with RPE-mIL2 or RPE-mIL2+aPD1 survived significantly longer than mice in the control groups (**Fig. 2H**). We did not observe any significant deviations in body weight overtime in any of the treatment groups suggesting that the therapy was well tolerated (Supplementary Fig. S3A–S3C). These results highlight the ability of RPE-mIL2 to act as a monotherapy and to boost the effectiveness of aPD1 checkpoint therapy when administered in combination.

A subset of the RPE-mIL2+aPD1–treated animals were evaluated for protection against recurrence in a rechallenge experiment. Briefly, animals treated with RPE-mIL2+aPD1 were challenged with a subcutaneous injection approximately 60 days after the initial intraperitoneal administration. 100% of previously treated mice were protected from recurrence and thus did not develop subcutaneous tumors while 5 of 6 control mice developed large tumors with evidence of necrosis (**Fig. 2I** and **J**) within the first 30 days. In addition, we did not observe any significant deviations in body weight in the rechallenged mice (Supplementary Fig. S3D and S3E). These results suggest that this treatment may provide immunologic memory against AB1 tumors which allows for protection against recurrence.

RPE-mIL2 and aPD1 combination treatment increased $CD4^+$ and $CD8^+$ T-cell activation, and RPE-mIL2 caused a phenotypic shift in macrophages from M2-like to M1-like

In this model, anti-PD1 checkpoint therapy is largely ineffective against AB1 tumors (Supplementary Fig. S4A). However, gene set enrichment analysis of a publicly available data set (accession no. GSE117358) revealed that the IL2 signaling pathway is associated with immunotherapy-responsive tumors (Supplementary Fig. S4B; ref. 46). For this reason, we hypothesized that RPE-mIL2 would work well as an antitumor therapeutic for mice with mesothelioma. We utilized CyTOF analysis to evaluate the changes in the presence and activation of various immune cells after treatment. Briefly, mice were stratified into 4 groups (Supplementary Fig. S5A and S5B) and treated with sham surgery, aPD1 injection, RPE-mIL2 only, or RPE-mIL2+aPD1.

We used Uniform Manifold Approximation and Projection (UMAP) dimension reduction to visualize the cellular landscape broadly (**Fig. 3A**) and with immune cell subset specificity (**Figs. 3C** and **4A**; Supplementary Fig. S6) of the intraperitoneal space after treatment. We found that there were no significant alterations in the total percentage of T cells or macrophages, but there were at least 4.4x fewer intraperitoneal B cells in mice treated with either RPE-mIL2 or RPE-mIL2+aPD1 when compared to sham treated mice (**Fig. 3B**). Notably, it has been reported that one of the most prevalent cells in the malignant mesothelioma tumor microenvironment is the immunoregulatory M2-like macrophage (47). We found a significant decrease in the percentage of M2-like macrophages ($CD86^-PD\text{-}L1^-$) after either RPE-mIL2 or RPE-mIL2+aPD1 combination treatment (**Fig. 3D**). Interestingly, we observed a corresponding increase in M1-like macrophages ($CD86^+PD\text{-}L1^+$) only in the mice treated with RPE-mIL2 (**Fig. 3D**) while the combination treated mice displayed a corresponding increase in conventional dendritic cells (cDC; $MHC\ II^+$; **Fig. 3E**). Furthermore, combination treatment resulted in significantly higher levels of CD40 from both macrophages and dendritic cells which further highlights the potential of RPE-mIL2 treatment to induce immunologic changes (**Fig. 3D** and **E**).

In addition to activating the adaptive immune system, we found that RPE-mIL2 and RPE-mIL2+aPD1–treated mice had 2.3x fewer naïve B cells and 1.9× more memory B cells than sham or aPD1–treated mice suggesting that RPE-mIL2 has a significant effect on B cell maturation (**Fig. 3F**). Further, we found notable changes in T cell subpopulations after administration of IL2 cytokine factories. Specifically, we found that RPE-mIL2 and RPE-mIL2+aPD1–treated mice had significantly fewer naïve ($CD69^-CD44^-CD62L^+$) $CD4^+$ and $CD8^+$ T cells as well as increased activated ($CD69^+CD44^+$) $CD4^+$ and $CD8^+$ T cells when compared with sham treated mice (**Fig. 4B** and **C**). Interestingly, RPE-mIL2 and RPE-mIL2+aPD1 caused 2× higher expression of proinflammatory IFNγ from activated $CD4^+$ T cells when compared to sham or aPD1 treatment (**Fig. 4B**). Taken together, these data suggest that combination therapy may boost the antitumor potential of both $CD4^+$ and $CD8^+$ T cells. Furthermore, RPE-mIL2 treatment caused a significant increase in $CD4^+$ and $CD8^+$ effector memory T cells ($CD69^-CD44^+CD62L^-$) when compared with sham mice (**Fig. 4B** and **C**) suggesting that our treatment was able to induce differentiation of critical T-cell subsets in mice with mesothelioma. Furthermore, we saw a 1.7x increase of PD-1 on $CD8^+$ T cells from mice treated with RPE-mIL2 when compared with the sham

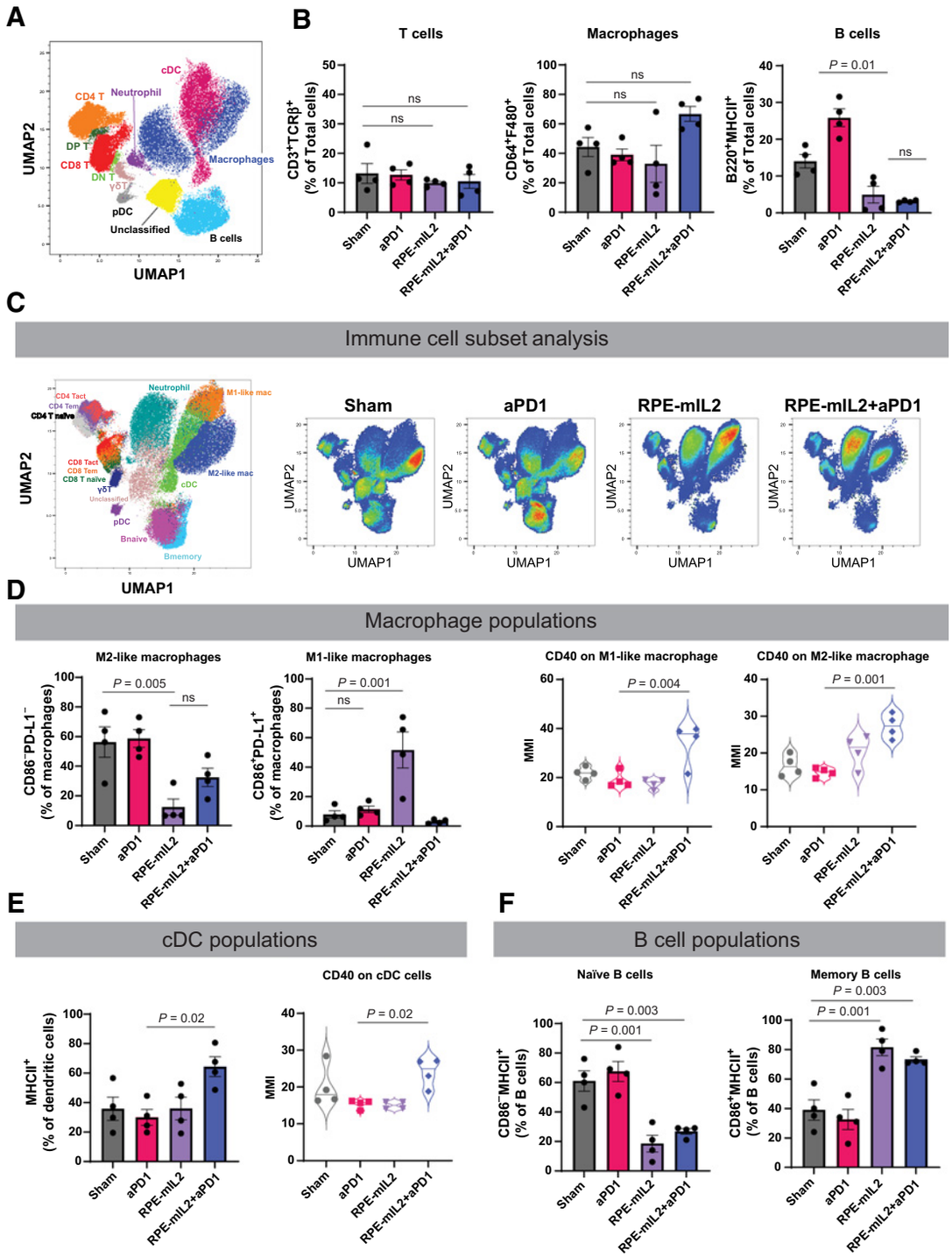

Figure 3.

Alteration of immune composition after RPE-mIL2 or RPE-mIL2+aPD1 therapy. **A,** Immune atlas map. We performed CyTOF with single cell suspension obtained from peritoneal lavage fluid. The Uniform Manifold Approximation and Projection (UMAP) was applied for dimensional reduction with 1,000,000 cells (40,000/each experiment × 4 mice/group × 4 groups). **B,** Comparison of T cells, macrophages, and B cells across treatment groups ($n = 4$ per group). **C,** UMAP of specific immune cell subsets. RPE-mIL2 treatment and combination of aPD1 therapy with mIL2 led to dramatic changes in lymphocytes and myeloid cell compositions. **D,** Comparison of M1-like and M2-like macrophages across treatment groups. Expression of CD40 among M1-like or M2-like macrophages across treatment groups. **E,** Comparison of cDC cells across treatment groups. Expression of CD40 among cDC cells across treatment groups. **F,** Comparison of naïve and memory B cells across treatment groups. *P* values were acquired using one-way ANOVA with Holm–Sidak method for multiple comparisons, ns = not significant.

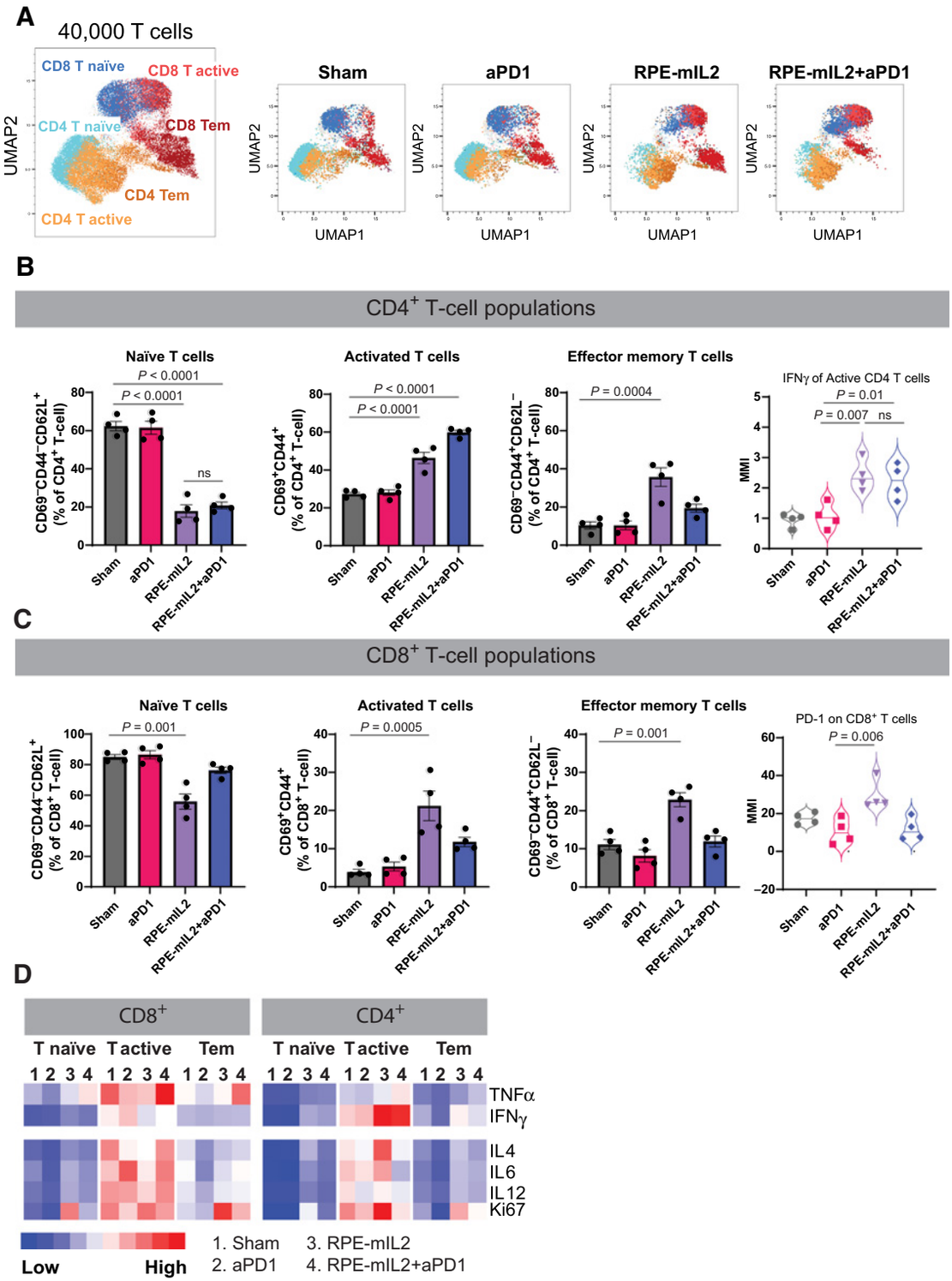

Figure 4.

Alteration of T-cell subsets after RPE-mIL2 or RPE-mIL2+aPD1 therapy. **A,** UMAP of specific T-cell subsets analyzed in this study. **B,** Comparison of naïve, activated, or effector memory CD4$^+$ T cells across treatment groups. Expression of IFNγ among activated CD4$^+$ T cells across treatment groups. **C,** Comparison of naïve, activated, or effector memory CD8$^+$ T cells across treatment groups. Expression of PD-1 among activated CD8$^+$ T cells across treatment groups ($n = 4$ per group). **D,** Heatmap of relative TNFα, IFNγ, IL4, IL6, IL12, and Ki67 expression across each group. *P* values were acquired using one-way ANOVA with Holm–Sidak method for multiple comparisons, ns = not significant.

group. This suggests a potential rationale for the success seen when used in combination with anti-PD1 therapy (**Fig. 4C**). Finally, we found high expression of TNFα, IL4, IL6, and IL12 as well as increased Ki67 proliferation marker on the T cells isolated from the RPE-mIL2 and combination treated mice (**Fig. 4D**). Taken together, these results suggest that RPE-mIL2 treatment has the potential to activate both innate and adaptive immune cells when administered in mice with AB1 tumors.

RPE-hIL2 can be safely administered to the intraperitoneal or pleural cavity and is well-tolerated in mice and rats

Before translating a product into clinical use, the safety and feasibility must be demonstrated. To address feasibility of dosing and the reproducibility of the foreign body response (FBR), we studied the *in vivo* pharmacokinetics of RPE-hIL2 in the intraperitoneal space of immunocompetent mice. The local (IP fluid) hIL2 concentration peaked by day 4 after implantation and declined at a rate inversely proportional to the pericapsular fibrotic overgrowth (PFO) accumulation on the surface of the capsules (Supplementary Fig. S7A and S7C) suggesting that PFO accumulation plays a role in RPE-hIL2 treatment duration. Notably, over 80% of the capsules implanted were retrieved at each time point (days 1, 4, 7, 14, 21, 47, and 60) highlighting the stability of the cytokine factories at physiological temperatures (Supplementary Fig. S7B). To assess the extent of fibrotic overgrowth and the stage/activity of the FBR for the RPE-hIL2 platform, we also examined the PFO at select time points (days 0, 4, 21, and 60) using H&E staining (Supplementary Fig. S7D). By day 60, a thick coating can clearly be seen encompassing the capsule(s), but the host cells on the surface of the capsules no longer possess distinct membranes and nuclei, thus demonstrating that the cells were not viable, the FBR remodeling was complete and the capsule-PFO particles were inert. All animals tolerated both the cell-delivered hIL2 and the alginate microcapsules at all-time points. This data was key for ensuring that the capsules: 1) did not continue to deliver cytokines after treatment completion and 2) did not pose a safety issue to the patients at extended periods.

To study the safety and translatability of hIL2 administration in the pleural cavity, we evaluated the effects of RPE-hIL2 (2 μg/day) in the pleural cavity of Sprague Dawley rats. First, we studied the pharmacodynamics of RPE-hIL2 administration and the ability of the host immune system to cause PFO accumulation on the surface of the cytokine factories when administered in the pleural cavity. Then we evaluated changes in the concentration of white blood cells (WBC), red blood cells (RBC), monocytes, and platelets in the blood. Finally, we evaluated the safety of this treatment via H&E staining, complete blood counts (CBC) and blood serum analysis. Notably, RPE-hIL2 cytokine factories were successfully administered to the pleural cavity in 20/20 rats (**Fig. 5A**) which highlights the feasibility of administration to this cavity. We found that hIL2 concentration peaked 24 hours after administration in the pleural fluid and the blood (**Fig. 5B**) and that the local concentration was at least 100× greater than the systemic concentration at all time points. This is critical for reducing off-target effects. Similar to the results seen in mice, the cytokine factories were heavily coated with pericapsular overgrowth by day 30 post-treatment (**Fig. 5C**). This observation corresponded with the reduction of hIL2 levels (local and systemic) back to pre-treatment levels and thus the hIL2 administration safely ended. Notably, we did not observe any significant deviations from control values in WBC, RBC, monocyte, or platelet concentrations at any time during our study. These data suggest that the cytokine factories were well tolerated by the host immune system.

Finally, our safety studies further highlight the clinical potential of this cytokine delivery platform. The liver, kidney, and lungs are often implicated in IL2-related toxicities (48) so we used H&E staining to assess the histopathologic condition of these organs 7, 21, or 30 days after RPE-hIL2 administration. Notably, we saw no major histopathologic changes in cells of the kidney, liver, lungs, or spleens when compared with control animals at the conclusion of our study (**Fig. 6A**). As expected, pleural IL2 altered the immune cell composition in the pleural cavity and peripheral lung. However, the rats were without adverse clinical events and demonstrated normal physical activity and respiratory function. The immune cell changes were resolved by day 21 without intervention as the therapy ceased secondary to the expected biomaterial response (Supplementary Fig. S8). In addition, we saw no significant changes in body weight, insulin levels, or glucose levels suggesting that the treatment was well tolerated (**Fig. 6B–D**). We saw a decrease in triglyceride levels 24 hours after administration, but this drop was transient and was managed by the animals without any intervention (**Fig. 6E**). Finally, we found no significant changes in high-density lipoprotein (HDL; **Fig. 6F**), low-density lipoprotein (LDL; **Fig. 6G**), alanine aminotransferase (ALT; **Fig. 6H**), or aspartate aminotransferase (AST; **Fig. 6I**) levels when compared to control animals which suggests healthy heart and liver function. In total, 20 of 20 rats dosed with RPE-hIL2 managed the cytokine factories without complication. To further highlight the translatability of this platform, we demonstrated the successful administration of cytokine factories via intrapleural catheters in porcine cadavers (Supplementary Fig. S9). Taken together, these data suggest that RPE-hIL2 can be safely and successfully administered to the pleural cavity and this work as a whole provides a rationale for translation into clinical studies for patients with pleural or intraperitoneal malignant mesothelioma.

Discussion

We recently developed and characterized a local delivery platform, called cytokine factories, composed of engineered RPE-mIL2 cells encapsulated in biocompatible alginate capsules to enable high dose IL2 administration for treatment of ovarian and colorectal cancers (41). Here, our IL2 cytokine factory was evaluated at increasing doses in an aggressive murine mesothelioma model. We determined that reduction in tumor burden correlated to RPE-mIL2 dose and that a dose of 5 μg/day RPE-mIL2 resulted in the most significant reduction in tumor burden (90%). Importantly, all doses were well tolerated with no observed fluctuations in weight over time. Furthermore, our platform was utilized in combination with the FDA-approved immune checkpoint inhibitor aPD1. 100% of AB1 tumors in the intraperitoneal space of mice treated with a combination of RPE-mIL2 and aPD1 were eradicated and did not recur upon rechallenge, suggesting the development of immunologic memory. CyTOF analysis of the intraperitoneal fluid of RPE-mIL2 and RPE-mIL2+aPD1–treated mice highlighted a reduction in CD86-PD-L1- M2-like macrophages, and a corresponding increase in $CD86^{+}PD\text{-}L1^{+}$ M1-like macrophages, and MHC II^{+} dendritic cells after treatment. Furthermore, treatment with our RPE-mIL2 cytokine factory as a monotherapy or alongside aPD1 resulted in fewer naïve $CD4^{+}$ and $CD8^{+}$ T cells and an increase in activated ($CD69^{+}CD44^{+}$) T cells. The changes in these cell populations highlight the involvement of both innate and adaptive immunity in the eradication of this cancer. Finally, we evaluated the pharmacokinetics and safety of this platform in the pleural cavity of Sprague Dawley rats, demonstrating 150× higher IL2 concentrations in the local compartment lasting 21–30 days. As intended, the capsules did

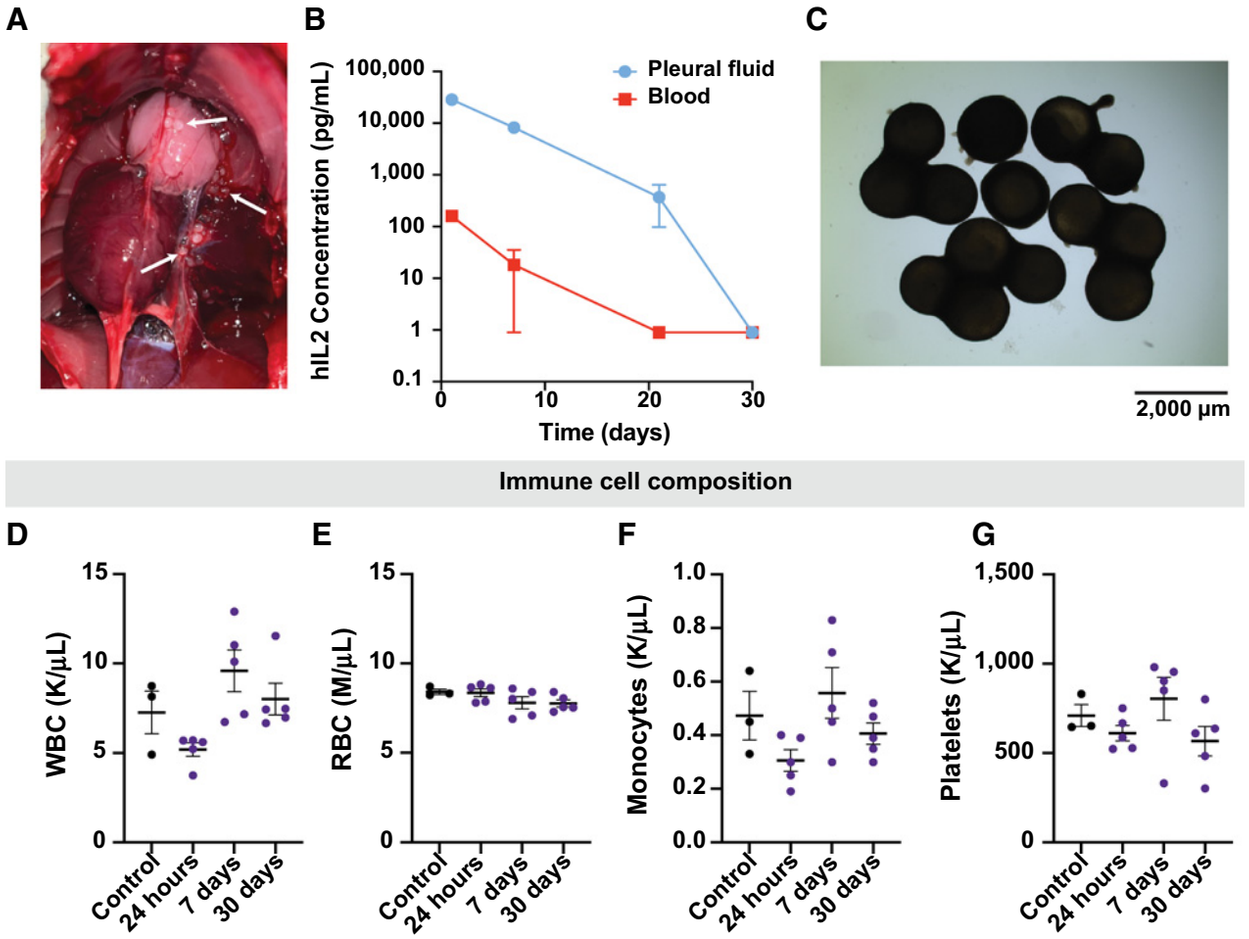

Figure 5.

Evaluation of human IL2 kinetics in the rat pleura. **A,** Macroscopic image of the pleural cavity 24 hours post implant. White arrows indicate RPE-hIL2. **B,** ELISA measurements of hIL2 concentration in the pleural cavity and blood at 24 hours, 7 days, 21 days, and 30 days post implant. **C,** Bright field images of capsules retrieved from the pleural cavity 30 days post implant. Image acquired at 2× magnification. **D-G,** Plots of white blood cell, red blood cell, monocyte, and platelet concentration derived from complete blood count analysis at 24 hours, 7 days, and 30 days post implant ($n = 5$ per group). Values are compared with untreated controls. Differences in cell concentration were not significant across all groups. *P* values were acquired using one-way ANOVA with Holm–Sidak method for multiple comparisons.

not degrade and were found to be biocompatible. Further, no persistent changes in complete blood cell counts or blood chemistry markers were observed.

As with many other cancers, cytotoxic chemotherapy is the standard treatment for patients with local or advanced malignant mesothelioma (49). However, malignant mesothelioma is a fibrotic tumor that is resistant to current approaches, including chemotherapy, radiation, and debulking (1, 9, 11–15, 17–22). Loss of immune control is commonly recognized as a hallmark of carcinogenesis, making the local delivery of immunotherapeutic agents an attractive alternative for treatment of this aggressive cancer (48). Immunotherapies offer an opportunity for long-term disease control that is not currently seen with chemotherapy. The IL2 cytokine factory described here is an approach that demonstrates drastic improvements in AB1 tumor burden in a safe and well-tolerated manner. Like other immunotherapies, including checkpoint inhibitors ipilimumab and nivolumab, the IL2 cytokine factory should be considered for patients with platinum-resistant tumors. The observed absence of tumor recurrence following rechallenge in cytokine factory treated groups also highlights the potential of this approach for patients who experience relapse. Importantly, immune checkpoint inhibitors are not effective in all patients, partly due to cytotoxic T-cell exhaustion. This phenomenon typically results in the loss of critical effector T-cell functions, such as IL2 production, high proliferative capacity, and cytotoxicity. Therefore, IL2 cytokine factories have the potential to act both as a monotherapy by inducing cytotoxicity and T-cell proliferation or as a means of enhancing immune checkpoint inhibitor efficacy through mediation of immune exhaustion (50).

To date, there are two FDA-approved cytokine therapies; high dose IL2 for metastatic melanoma and renal carcinoma and IFNα for stage III melanoma. However, cytokines as monotherapies have not been widely effective across all patients due to dose-limiting toxicities that prevent patients from completing the full course of therapy (34, 51–53). Currently, many commercialized cytokines are recombinantly produced cytokine variants engineered to improve bioactivity and function mainly by increasing protein stability (52). Other modifications have also been implemented, such as antibody-fused cytokines that enhance localization and conjugation with poly(ethylene glycol)

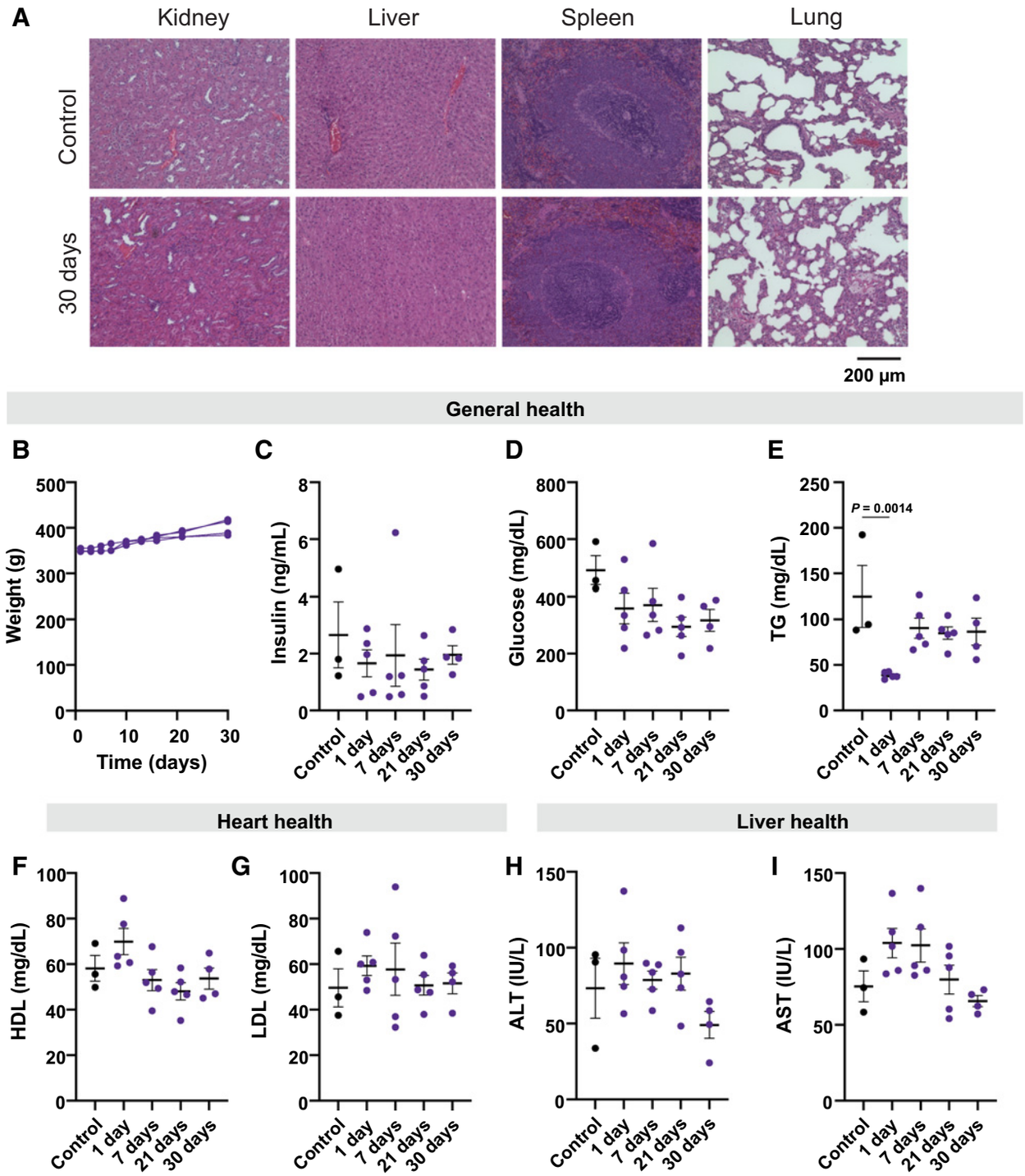

Figure 6.

Toxicological analysis of hIL2 in the rat pleura over the span of 30 days. **A,** Representative images of H&E-stained sections of the kidney, liver, spleen, and lungs of untreated control rats compared with rats sacrificed at 30 days post capsule implant ($n = 5$). **B,** Plot tracking the weight of individual rats over the course of treatment. **C** and **D,** Evaluation of general health through changes in insulin and glucose for each time point. Values are compared with untreated controls. Differences in values were not significant across all groups. *P* values were acquired using one-way ANOVA with Holm–Sidak method for multiple comparisons. **E,** Evaluation of general health through changes in triglycerides for each time point. **F** and **G,** Evaluation of heart health through changes in HDL and LDL levels over time. **H** and **I,** Evaluation of liver health through changes in ALT and AST levels over time. All values are compared with untreated controls. Differences in values were not significant across all groups. *P* values were acquired using one-way ANOVA with Holm–Sidak method for multiple comparisons.

(PEG) which functions to improve pharmacokinetics (54). Though these techniques have been able to resolve limitations of toxicity, each is associated with reduced efficacy. Modified cytokines are typically less potent and are limited in the number of doses that can be administered (55). Furthermore, various properties of the PEG polymer can modify the interaction capabilities of the bound protein and have been shown to affect biological activity and bioavailability (56, 57). The results of this study as well as our previous work demonstrate that native IL2 produced from RPE cells maintain bioactivity. In addition, the encapsulation of these cells within a hydrogel matrix and subsequent local administration enables the delivery of physiologically relevant concentrations of IL2 directly to the tumor without cytotoxicity, which is often observed with traditional cytokine therapies.

While this approach has significant potential, unlike recombinant IL2 cytokines, which are typically injected, the relatively large size of the cytokine factory prevents it from being administered non-invasively. However, patients receiving treatment for malignant mesothelioma often require chest catheter placement for drainage of pleural effusions throughout the course of treatment. This is done in outpatient settings and can be used in a similar manner to administer RPE-IL2. Thus, recovery time is not significantly increased through the administration of RPE-IL2. Furthermore, it has been demonstrated that local IL2 reduces malignant pleural effusions in 81% of patients (58). This advantage of local IL2 delivery results in a less frequent need for fluid drainage throughout treatment leading to a significant improvement in patient quality of life.

Overall, we observed a significant reduction of tumor burden in mice treated with RPE-mIL2 monotherapy and complete eradication of tumor burden in mice treated with RPE-mIL2 and aPD1 combination therapy. This effect was achieved through the modulation of both innate and adaptive immune populations and was accompanied by protection against tumor recurrence. Importantly, immune activation was attained while mitigating prolonged toxicity in both peritoneal and pleural cavities. Although previous studies have demonstrated that IL2 is highly efficacious, our cytokine factory is the first approach that requires minimal access to the target site. This advantage overcomes current clinical drawbacks regarding catheter infection and may alleviate overall adverse events. The continued occurrence of malignant mesothelioma necessitates the clinical assessment of new, effective treatments. Thus, the potential of the IL2 cytokine factory described here to ease the global burden of malignant mesothelioma highlights the urgency of its evaluation in clinical trials.

Authors' Disclosures

A.M. Nash reports grants from Avenge Bio and National Science Foundation during the conduct of the study as well as personal fees from Avenge Bio outside the submitted work; in addition, A.M. Nash has a patent for materials and formulations thereof licensed and with royalties paid from Avenge Bio, a patent for method for improved delivery licensed and with royalties paid from Avenge Bio, a patent for rapid platform for cell-based vaccination licensed and with royalties paid from Avenge Bio, a patent for encapsulated cells expressing IL-12 and uses thereof licensed and with royalties paid from Avenge Bio, a patent for encapsulated cells expressing IL2 and uses thereof licensed and with royalties paid from Avenge Bio, and a patent for methods of use and administration of encapsulated cells licensed and with royalties paid from Avenge Bio. S. Aghlara-Fotovat reports grants from Avenge Bio during the conduct of the study; in addition, S. Aghlara-Fotovat has a patent for materials and formulations thereof licensed and with royalties paid from Avenge Bio, a patent for encapsulated cells expressing IL-12 and uses thereof licensed and with royalties paid from Avenge Bio, a patent for encapsulated cells expressing IL2 and uses thereof licensed and with royalties paid from Avenge Bio, and a patent for methods of use and administration of encapsulated cells licensed and with royalties paid from Avenge Bio. H.-S. Lee reports grants from the Cancer Prevention and Research Institute of Texas (PI), National Institutes of Health (NIH), and Samyang Biopharmaceutical USA during the conduct of the study. B.M. Burt reports grants from Cancer Prevention Research Institute of Texas during the conduct of the study as well as grants from AstraZeneca, Novartis, Momotero-Gene, NIH, and Cancer Prevention and Research Institute of Texas and personal fees from Intuitive Surgical outside the submitted work. R.K. Ghanta reports personal fees from Avenge Bio during the conduct of the study as well as personal fees from Avenge Bio outside the submitted work. O. Veiseh reports grants, personal fees, and nonfinancial support from Avenge Bio during the conduct of the study as well as grants, personal fees, and nonfinancial support from Avenge Bio outside the submitted work. In addition, O. Veiseh has a patent for cytokine factories pending, licensed, and with royalties paid from Avenge Bio; a patent for materials and formulations thereof licensed and with royalties paid from Avenge Bio; a patent for a method for improved delivery licensed and with royalties paid from Avenge Bio; a patent for rapid platform for cell-based vaccination licensed and with royalties paid from Avenge Bio; a patent for encapsulated cells expressing IL-12 and uses thereof licensed and with royalties paid from Avenge Bio; a patent for encapsulated cells expressing IL2 and uses thereof licensed and with royalties paid from Avenge Bio; and a patent for methods of use and administration of encapsulated cells licensed and with royalties paid from Avenge Bio. No disclosures were reported by the other authors.

Authors' Contributions

A.M. Nash: Conceptualization, resources, data curation, software, formal analysis, validation, investigation, visualization, methodology, writing–original draft, writing–review and editing. **S. Aghlara-Fotovat:** Conceptualization, resources, data curation, software, formal analysis, validation, investigation, visualization, methodology, writing–original draft, writing–review and editing. **B. Castillio:** Resources, data curation, formal analysis, investigation, visualization, methodology. **A. Hernandez:** Resources, data curation, formal analysis, investigation, visualization, methodology. **A. Pugazenthi:** Data curation, investigation, visualization, methodology. **H.-S. Lee:** Resources, software, formal analysis, investigation, visualization, methodology, writing–review and editing. **H.-J. Jang:** Resources, data curation, software, formal analysis, validation, investigation, visualization, methodology, writing–review and editing. **A. Nguyen:** Investigation, visualization, methodology. **A. Lu:** Investigation, methodology. **B.M. Burt:** Conceptualization, data curation, software, supervision, funding acquisition, validation, investigation, visualization, methodology, project administration, writing–review and editing. **R.K. Ghanta:** Data curation, formal analysis, validation, investigation, visualization, methodology, project administration, writing–review and editing. **O. Veiseh:** Conceptualization, resources, formal analysis, supervision, funding acquisition, investigation, visualization, methodology, project administration, writing–review and editing.

Acknowledgments

Cancer Prevention Research Institute of Texas grant RR160047 (to O. Veiseh), National Science Foundation grant 1842494 (to A.M. Nash), National Institute of Health grant 1R01DK120459-01 (to A.M. Nash, O. Veiseh). The authors would like to acknowledge the Mouse Metabolism and Phenotyping Core at Baylor College of Medicine for assistance with toxicity analysis.

The publication costs of this article were defrayed in part by the payment of publication fees. Therefore, and solely to indicate this fact, this article is hereby marked "advertisement" in accordance with 18 USC section 1734.

Note

Supplementary data for this article are available at Clinical Cancer Research Online (http://clincancerres.aacrjournals.org/).

Received May 10, 2022; revised June 21, 2022; accepted August 12, 2022; published first September 12, 2022.

References

1. Nelson DB, Rice DC, Niu J, Atay S, Vaporciyan AA, Antonoff M, et al. Long-term survival outcomes of cancer-directed surgery for malignant pleural mesothelioma: propensity score matching analysis. J Clin Oncol 2017;35:3354–62.
2. Meyerhoff RR, Yang CF, Speicher PJ, Gulack BC, Hartwig MG, D'Amico TA, et al. Impact of mesothelioma histologic subtype on outcomes in the surveillance, epidemiology, and end results database. J Surg Res 2015;196:23–32.

3. Musk AW, Olsen N, Alfonso H, Reid A, Mina R, Franklin P, et al. Predicting survival in malignant mesothelioma. Eur Respir J 2011;38:1420–4.
4. Linton A, Pavlakis N, O'Connell R, Soeberg M, Kao S, Clarke S, et al. Factors associated with survival in a large series of patients with malignant pleural mesothelioma in New South Wales. Br J Cancer 2014;111:1860–9.
5. Taioli E, Wolf AS, Camacho-Rivera M, Kaufman A, Lee DS, Nicastri D, et al. Determinants of survival in malignant pleural mesothelioma: a surveillance, epidemiology, and end results (SEER) Study of 14,228 patients. PLoS One 2015;10:e0145039.
6. Robinson BM. Malignant pleural mesothelioma: an epidemiological perspective. Ann Cardiothorac Surg 2012;1:491–6.
7. Carbone M, Kratzke RA, Testa JR. The pathogenesis of mesothelioma. Semin Oncol 2002;29:2–17.
8. Goodman JE, Nascarella MA, Valberg PA. Ionizing radiation: a risk factor for mesothelioma. Cancer Causes Control 2009;20:1237–54.
9. Vogelzang NJ, Rusthoven JJ, Symanowski J, Denham C, Kaukel E, Ruffie P, et al. Phase III study of pemetrexed in combination with cisplatin versus cisplatin alone in patients with malignant pleural mesothelioma. J Clin Oncol 2003;21:2636–44.
10. Zalcman G, Mazieres J, Margery J, Greillier L, Audigier-Valette C, Moro-Sibilot D, et al. Bevacizumab for newly diagnosed pleural mesothelioma in the mesothelioma avastin cisplatin pemetrexed study (MAPS): a randomised, controlled, open-label, phase 3 trial. Lancet 2016;387:1405–14.
11. Boutin C, Rey F, Viallat JR. Prevention of malignant seeding after invasive diagnostic procedures in patients with pleural mesothelioma. A randomized trial of local radiotherapy. Chest 1995;108:754–8.
12. Rusch VW, Rosenzweig K, Venkatraman E, Leon L, Raben A, Harrison L, et al. A phase II trial of surgical resection and adjuvant high-dose hemithoracic radiation for malignant pleural mesothelioma. J Thorac Cardiovasc Surg 2001;122:788–95.
13. Gomez DR, Hong DS, Allen PK, Welsh JS, Mehran RJ, Tsao AS, et al. Patterns of failure, toxicity, and survival after extrapleural pneumonectomy and hemithoracic intensity-modulated radiation therapy for malignant pleural mesothelioma. J Thorac Oncol 2013;8:238–45.
14. Rice DC, Stevens CW, Correa AM, Vaporciyan AA, Tsao A, Forster KM, et al. Outcomes after extrapleural pneumonectomy and intensity-modulated radiation therapy for malignant pleural mesothelioma. Ann Thorac Surg 2007;84:1685–92; discussion 92–3.
15. Sugarbaker DJ, Richards WG, Bueno R. Extrapleural pneumonectomy in the treatment of epithelioid malignant pleural mesothelioma: novel prognostic implications of combined N1 and N2 nodal involvement based on experience in 529 patients. Ann Surg 2014;260:577–80; discussion 80–2 [pii].
16. Rusch VW, Giroux D, Kennedy C, Ruffini E, Cangir AK, Rice D, et al. Initial analysis of the international association for the study of lung cancer mesothelioma database. J Thorac Oncol 2012;7:1631–9.
17. Burt BM, Cameron RB, Mollberg NM, Kosinski AS, Schipper PH, Shrager JB, et al. Malignant pleural mesothelioma and the society of thoracic surgeons database: an analysis of surgical morbidity and mortality. J Thorac Cardiovasc Surg 2014;148:30–5.
18. Zellos L, Richards WG, Capalbo L, Jaklitsch MT, Chirieac LR, Johnson BE, et al. A phase I study of extrapleural pneumonectomy and intracavitary intraoperative hyperthermic cisplatin with amifostine cytoprotection for malignant pleural mesothelioma. J Thorac Cardiovasc Surg 2009;137:453–8.
19. Neragi-Miandoab S, Richards WG, Sugarbaker DJ. Morbidity, mortality, mean survival, and the impact of histology on survival after pleurectomy in 64 patients with malignant pleural mesothelioma. Int J Surg 2008;6:293–7.
20. Tilleman TR, Richards WG, Zellos L, Johnson BE, Jaklitsch MT, Mueller J, et al. Extrapleural pneumonectomy followed by intracavitary intraoperative hyperthermic cisplatin with pharmacologic cytoprotection for treatment of malignant pleural mesothelioma: a phase II prospective study. J Thorac Cardiovasc Surg 2009;138:405–11.
21. Sugarbaker DJ, Jaklitsch MT, Bueno R, Richards W, Lukanich J, Mentzer SJ, et al. Prevention, early detection, and management of complications after 328 consecutive extrapleural pneumonectomies. J Thorac Cardiovasc Surg 2004;128:138–46.
22. Sugarbaker DJ, Gill RR, Yeap BY, Wolf AS, DaSilva MC, Baldini EH, et al. Hyperthermic intraoperative pleural cisplatin chemotherapy extends interval to recurrence and survival among low-risk patients with malignant pleural mesothelioma undergoing surgical macroscopic complete resection. J Thorac Cardiovasc Surg 2013;145:955–63.
23. Scherpereel A, Mazieres J, Greillier L, Lantuejoul S, Do P, Bylicki O, et al. Nivolumab or nivolumab plus ipilimumab in patients with relapsed malignant pleural mesothelioma (IFCT-1501 MAPS2): a multicentre, open-label, randomised, non-comparative, phase 2 trial. Lancet Oncol 2019;20:239–53.
24. Baas P, Scherpereel A, Nowak AK, Fujimoto N, Peters S, Tsao AS, et al. First-line nivolumab plus ipilimumab in unresectable malignant pleural mesothelioma (CheckMate 743): a multicentre, randomised, open-label, phase 3 trial. Lancet 2021;397:375–86.
25. Alley EW, Lopez J, Santoro A, Morosky A, Saraf S, Piperdi B, et al. Clinical safety and activity of pembrolizumab in patients with malignant pleural mesothelioma (KEYNOTE-028): preliminary results from a non-randomised, open-label, phase 1b trial. Lancet Oncol 2017;18:623–30.
26. Quispel-Janssen J, van der Noort V, de Vries JF, Zimmerman M, Lalezari F, Thunnissen E, et al. Programmed death 1 blockade with nivolumab in patients with recurrent malignant pleural mesothelioma. J Thorac Oncol 2018;13:1569–76.
27. Metaxas Y, Rivalland G, Mauti LA, Klingbiel D, Kao S, Schmid S, et al. Pembrolizumab as palliative immunotherapy in malignant pleural mesothelioma. J Thorac Oncol 2018;13:1784–91.
28. Kindler HKT, Carol Tan Y. Rose B, Ahmad M, Straus C, Sargis R, et al. OA13.02 phase II trial of pembrolizumab in patients with malignant mesothelioma (MM): interim analysis. J Thorac Oncol 2017;12:S293–S4.
29. Janes SM, Alrifai D, Fennell DA. Perspectives on the treatment of malignant pleural mesothelioma. N Engl J Med 2021;385:1207–18.
30. Wright K. FDA approves nivolumab plus ipilimumab for previously untreated unresectable malignant pleural mesothelioma. Oncology 2020;34:502–3.
31. Johnson DB, Balko JM, Compton ML, Chalkias S, Gorham J, Xu Y, et al. Fulminant myocarditis with combination immune checkpoint blockade. N Engl J Med 2016;375:1749–55.
32. Dougan M, Pietropaolo M. Time to dissect the autoimmune etiology of cancer antibody immunotherapy. J Clin Invest 2020;130:51–61.
33. Riley RS, June CH, Langer R, Mitchell MJ. Delivery technologies for cancer immunotherapy. Nat Rev Drug Discov 2019;18:175–96.
34. Berraondo P, Sanmamed MF, Ochoa MC, Etxeberria I, Aznar MA, Perez-Gracia JL, et al. Cytokines in clinical cancer immunotherapy. Br J Cancer 2019;120:6–15.
35. Den Otter W, Jacobs JJ, Battermann JJ, Hordijk GJ, Krastev Z, Moiseeva EV, et al. Local therapy of cancer with free IL2. Cancer Immunol Immunother 2008;57:931–50.
36. Goey SH, Eggermont AM, Punt CJ, Slingerland R, Gratama JW, Oosterom R, et al. Intrapleural administration of interleukin 2 in pleural mesothelioma: a phase I-II study. Br J Cancer 1995;72:1283–8.
37. Castagneto B, Zai S, Mutti L, Lazzaro A, Ridolfi R, Piccolini E, et al. Palliative and therapeutic activity of IL2 immunotherapy in unresectable malignant pleural mesothelioma with pleural effusion: Results of a phase II study on 31 consecutive patients. Lung Cancer 2001;31:303–10.
38. Astoul P, Picat-Joossen D, Viallat JR, Boutin C. Intrapleural administration of interleukin-2 for the treatment of patients with malignant pleural mesothelioma: a Phase II study. Cancer 1998;83:2099–104.
39. Zhang YT, Zhong XD, Gao YL, Chang J. Evaluation of IL2 and Dexamethasone intracavitary injection on the management of malignant effusion in children with solid tumors or lymphoma. BMC Cancer 2021;21:1302.
40. Donnenberg AD, Luketich JD, Dhupar R, Donnenberg VS. Treatment of malignant pleural effusions: the case for localized immunotherapy. J Immunother Cancer 2019;7:110.
41. Nash AM, Jarvis MI, Aghlara-Fotovat S, Mukherjee S, Hernandez A, Hecht AD, et al. Clinically translatable cytokine delivery platform for eradication of intraperitoneal tumors. Sci Adv 2022;8:eabm1032.
42. Ghanta RK, Aghlara-Fotovat S, Pugazenthi A, Ryan CT, Singh VP, Mathison M, et al. Immune-modulatory alginate protects mesenchymal stem cells for sustained delivery of reparative factors to ischemic myocardium. Biomater Sci 2020;8:5061–70.
43. Becht E, McInnes L, Healy J, Dutertre CA, Kwok IWH, Ng LG, et al. Dimensionality reduction for visualizing single-cell data using UMAP. Nat Biotechnol 2018.
44. Liao W, Lin JX, Leonard WJ. Interleukin-2 at the crossroads of effector responses, tolerance, and immunotherapy. Immunity 2013;38:13–25.
45. Liao D, Yu Y, Mei Q, Wang Z, Li X, Jia Y, et al. Advances in immunotherapy of malignant pleural mesothelioma. Onco Targets Ther 2021;14:4477–84.
46. Zemek RM, De JE, Chin WL, Schuster IS, Fear VS, Casey TH, et al. Sensitization to immune checkpoint blockade through activation of a STAT1/NK axis in the tumor microenvironment. Sci Transl Med 2019;11:eaav7816.

47. Desage AL, Karpathiou G, Peoc'h M, Froudarakis ME. The immune microenvironment of malignant pleural mesothelioma: a literature review. Cancers 2021; 13:3205.
48. Adusumilli PS, Zauderer MG, Riviere I, Solomon SB, Rusch VW, O'Cearbhaill RE, et al. A phase I trial of regional mesothelin-targeted CAR T-cell therapy in patients with malignant pleural disease, in combination with the anti-PD-1 agent pembrolizumab. Cancer Discov 2021;11:2748–63.
49. Banerji S, Meyers DE, Harlos C, Dawe DE. The role of immunotherapy in the treatment of malignant pleural mesothelioma. Curr Oncol 2021;28: 4542–51.
50. Wherry EJ. T cell exhaustion. Nat Immunol 2011;12:492–9.
51. Qiao J, Fu YX. Cytokines that target immune killer cells against tumors. Cell Mol Immunol 2020;17:722–7.
52. Pires IS, Hammond PT, Irvine DJ. Engineering strategies for immunomodulatory cytokine therapies - challenges and clinical progress. Adv Ther 2021;4: 2100035.
53. Xue D, Hsu E, Fu YX, Peng H. Next-generation cytokines for cancer immunotherapy. Antib Ther 2021;4:123–33.
54. Charych DH, Hoch U, Langowski JL, Lee SR, Addepalli MK, Kirk PB, et al. NKTR-214, an engineered cytokine with biased IL2 receptor binding, increased tumor exposure, and marked efficacy in mouse tumor models. Clin Cancer Res 2016;22:680–90.
55. Mizui M. Natural and modified IL2 for the treatment of cancer and autoimmune diseases. Clin Immunol 2019;206:63–70.
56. Zhang F, Liu MR, Wan HT. Discussion about several potential drawbacks of PEGylated therapeutic proteins. Biol Pharm Bull 2014;37:335–9.
57. Veronese FM, Mero A. The impact of PEGylation on biological therapies. BioDrugs 2008;22:315–29.
58. Yasumoto K, Mivazaki K, Nagashima A, Ishida T, Kuda T, Yano T, et al. Induction of lymphokine-activated killer cells by intrapleural instillations of recombinant interleukin-2 in patients with malignant pleurisy due to lung cancer. Cancer Res 1987;47:2184–7.